Effect of heat integration method and torrefaction temperature on the performance of an integrated CHP-torrefaction plant

Sermyagina Ekaterina, Saari Jussi, Zakeri Behnam, Kaikko Juha, Vakkilainen Esa

DOI: 10.1016/j.apenergy.2015.03.102

Please cite the publication as follows:

Sermyagina, E., Saari, J., Zakeri, B., Kaikko, J., Vakkilainen, E. (2015). Effect of heat integration method and torrefaction temperature on the performance of an integrated CHP-torrefaction plant. Applied Energy, Vol. 149, pp. 24-34. DOI: 10.1016/j.apenergy.2015.03.102

Effect of heat integration method and torrefaction temperature on the performance of an integrated CHP-torrefaction plant

Ekaterina Sermyagina[a,*], Jussi Saari[a], Behnam Zakeri[b], Juha Kaikko[a], Esa Vakkilainen[a]
[a] Lappeenranta University of Technology, Lappeenranta, Finland
[b] Aalto University, Helsinki, Finland

Abstract: An important factor for industrial-scale implementation of torrefaction – a thermal pre-treatment technology that enhances the fuel characteristics of biomass – is the requirement for a low-cost source of heat energy. Significant benefits can be achieved if torrefaction is integrated with a large heat producer. To study this possibility, a new model for the energy and mass balances of the torrefaction process was developed on the basis of available experimental data. The torrefaction model was then integrated into steam power plant simulations, and the performance of different integration schemes was evaluated. To investigate the effect of plant size and operating mode, the same configurations were studied for both large and small combined heat and power (CHP) plants. Large plant operates at full boiler load, and capturing of a certain heat from plant cycle reduces the power output for all integration cases. At the same time, higher trigeneration efficiencies in comparison with non-integrated case together with fuel consumption decrease due to torrefaction gas co-firing indicate that integration of torrefaction and CHP plant at full load could be beneficial. In case of small plant, free boiler capacity at reduced-load conditions allows to cover the torrefaction heat demand and simultaneously increase the electricity generation for almost all integration cases. Trigeneration efficiency is changing within a relatively narrow range for most of the cases, while the solid fuel consumption is higher than in design case. This work shows that integration method together with process temperature and plant operation mode are the important factors that could have a diverse effect on CHP plant integration with torrefaction process.

Keywords: torrefaction; biomass; modeling; integration; CHP

1. Introduction

Many different types of biomass are available, for example, agricultural residues, herbaceous crops and the material most commonly used in industry, woody biomass. Wood has a number of properties that make it suitable for energy production; the comparatively high energy content, the low demand for fertilizers and herbicides, and the high yield per land area [1]. On the other hand, wood as such has several shortcomings, for example, low density, high moisture content, a hydrophilic nature, poor grindability and inconsistent quality. These characteristics increase transport, storage and handling costs, limiting possible applications [2]. Torrefaction, also known as roasting or mild pyrolysis, is a form of thermochemical treatment that improves some of the unfavourable properties of biomass as a fuel. In the torrefaction process, biomass is heated in an inert atmosphere at 200–300 ºC, losing mass and energy with the gas produced. The remaining solid product is more brittle and hydrophobic than the original material [1-3], and subsequent pelletizing of the torrefied wood yields a product with high energy density. Several studies have reported positive results on the technical and economic feasibility of torrefied pellet production [4–6]. Small-scale pellet combustion for heating, entrained-flow gasification, replacement of coal or co-firing in coal-fired power plants have all been proposed as potential uses for torrefied pellets [1, 5–7].

Woody biomass is a quite important commodity, and its role increases in many spheres worldwide. The global solid biofuel trade, consisting mainly of forest wood biomass, experienced a nearly six-fold growth from 56 to 300 PJ annually in the decade 2000–2010 [8]. According to the International Energy Agency ‘BLUE Map’ scenario, to attain a clean yet competitive energy supply, biomass use for energy would have to increase three-fold by 2050 compared with levels in 2005 [9].The European Union is promoting the use of renewable energy, including biomass, and is encouraging a decrease in primary energy consumption through improved efficiency in energy generation, transmission and end-use. Directive 2012/27/EU offers comprehensive measures for reaching the EU’s 20% energy efficiency target by 2020 [10]. Solid biofuel with improved properties can substitute a higher share of coal in coal-fired plants: while a co-firing rate of less than 20% of energy content is currently assumed feasible for untreated biomass in coal-fired plants, torrefied biomass can replace more than 50% of the coal fuel [11, 12].

* Corresponding author. Tel.: +358 469067661
E-mail address: Ekaterina.Sermyagina@lut.fi (E. Sermyagina).

Optimal heat integration of biomass conversion into power production thus offers a potentially valuable approach that can contribute considerably to meeting goals for the energy supply of the future.

The torrefaction process requires heat for both drying of the biomass and the torrefaction itself. In addition to the torrefied biomass, the process produces a fuel gas stream as a side product and waste heat from cooling of the torrefied solid product. A biomass-fired combined heat and power (CHP) plant is in many ways an excellent candidate for integration with the torrefaction process as the feedstock logistics, storage and handling facilities already exist, and potential heat sources and sinks for heating and cooling needs are available.

A number of studies of polygeneration systems that integrate CHP plants with various biomass conversion technologies have been published. Studies have found benefits in integrating ethanol production [13–17], gasification [18–20] or pelletization [21] with existing CHP plants. Kohl et al. [22] compared pelletization, torrefaction and pelletization, and fast pyrolysis integrated with a CHP plant, concluding that energy efficiency improved as a result of the increased yearly boiler workload in comparison with stand-alone operation.

Reported data on combining torrefaction with CHP plants is, however, limited. An investigation of an integration case with a 120 MW_{th} CHP has been presented by Håkansson et al. [23]. In another study, Li et al. [24] investigated the potential and effects of co-firing torrefied biomass in a coal-fired boiler. The impacts of various integration concepts of the CHP plant and torrefaction process have, however, not been studied in detail. In addition, the question of CHP plant size has not received proper attention. Research on the most favorable economic and technical integration concept is of considerable interest since the results are applicable also to currently operating plants. In view of the significant consumption of woody biomass by the pulp and paper industry, e.g. in the Nordic area, the development and integration of torrefaction into the CHP cycle is deemed to have an essential potential.

The aim of this study is to investigate different integration concepts and the effect of plant size on the thermodynamic performance of a CHP-torrefaction polygeneration system. A mass and energy balance model is created to predict solid- and gas-phase mass yields and heating values on the basis of published experimental data on the torrefaction of typical Scandinavian wood biomasses (pine, spruce, birch, and mixed-species logging residues). Development of the models is described and results of simulation of the integration scenarios are presented.

2. Modeling of torrefaction

2.1. Model development

IPSEpro process simulation software [25] was used to investigate integration of the torrefaction process into CHP plants. The software does not offer a ready-made torrefaction process model, but does provide standard CHP plant components and includes a model development kit to design new process components to complement the standard component library.

The industrial-type torrefaction equipment considered consists of three parts: a dryer, torrefaction reactor, and cooler for the solid product. Indirect heating and cooling are assumed, but detailed component operation is not considered. The gas-phase product is directed to combustion, e.g., in a boiler or furnace. Figure 1 shows a schematic diagram of the developed model.

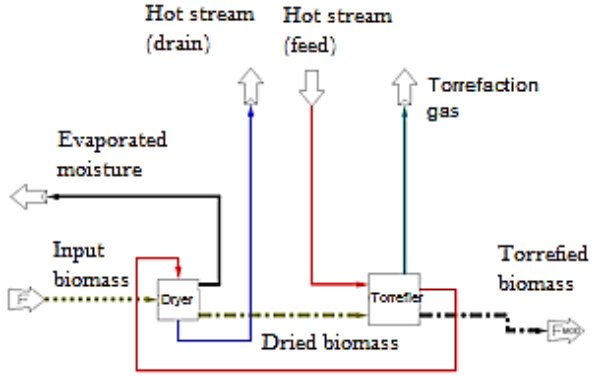

Fig. 1. Torrefaction process model in IPSEpro software.

2.2. Torrefaction products

The main components of wood are three polymeric structures: hemicellulose, cellulose and lignin, of which mainly hemicellulose is affected by torrefaction. Torrefaction occurs at a temperature range of 200…300 ºC. At temperatures below 250 ºC, hemicellulose devolatilization and carbonization are limited, but at higher temperatures, decomposition of all the main components becomes extensive as lignin and cellulose also begin limited devolatilization below 300 ºC [26]. Mass loss increases with time, but based on experiments with willow, beech and spruce, the rate of mass loss slows down considerably after the first 20 to 30 minutes [27, 28].

Solid product mass and energy yields of 70% and 90%, respectively, for a 30% increase in LHV are often quoted, citing the report by Bergman et al. [6], but somewhat lower energy retention appears more common in most experiments with European woods. The results are quite diverse, ranging from 95.1% and 96.5% (willow, [32]) to 52% and 71% (pine, [30]) for mass and energy yields, respectively. Figure 2 summarizes a selection of published yields from torrefaction experiments with pine [29, 30], birch [29], spruce [31], willow [32], wood briquettes [33], and logging residues [30].

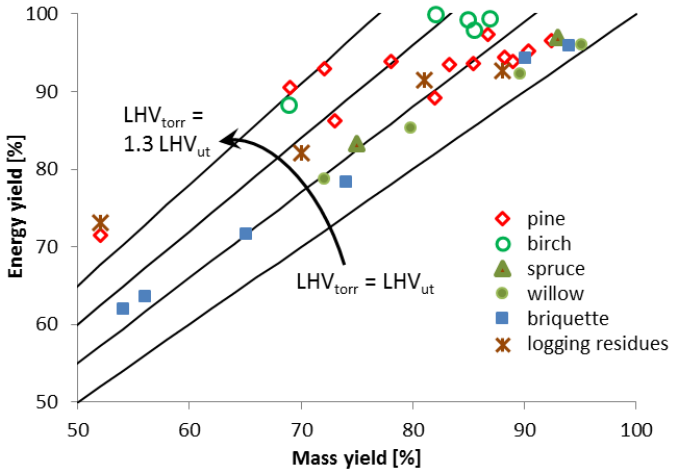

Fig. 2. Mass and energy yields for torrefaction of different wood biomasses [29–33]. The lines represent the increase in torrefied product heating value LHV_{torr} relative to untreated feed LHV_{ut} (both dry, ash-free).

The torrefaction model used in this study is based on an assumption that the sum of the available energy of feedstock dry matter and heat of reaction is divided between available heats of the gaseous and solid products:

$$\dot{m}_{\mathrm{d}}\left(LHV_{\mathrm{d}} + h_{\mathrm{react}}\right) = \dot{m}_{\mathrm{g}} LHV_{\mathrm{g}} + \dot{m}_{\mathrm{torr}} LHV_{\mathrm{torr}} \quad (1)$$

where h_{react} [kJ/kg] is the heat of reaction; $\dot{m}_d$, $\dot{m}_g$ and $\dot{m_{torr}}$ [kg/s] are the mass flows of feedstock dry matter, torrefaction gas and torrefied biomass; LHV_d, LHV_g and LHV_{torr} [MJ/kg] are their lower heating values correspondingly.

Available data on the parameters of interest – mass yield, gaseous product heating value, and solid product heating value – suffer from being somewhat limited and from being dispersed among references using different assumptions, measurement approaches, and experimental parameters.

To close the energy balance, solid product mass yield, gas heating value, and heat of reaction were estimated on the basis of published experimental results. Solid product heating value was then solved using Eq. (1). This approach was considered necessary, because being roughly an order of magnitude less than the solid product heating value, the gas-phase heating value would otherwise be subject to potentially very large relative errors from comparatively uncertain solid product LHV estimates.

The mass yield M [-], or ratio of solid product to feedstock dry fraction, was determined from the correlation expressed in Eq. (2).

$$M = \frac{m_{\mathrm{torr}}}{m_{\mathrm{d}}} = 1 - a(T_{\mathrm{torr}} - T_{\mathrm{ini}})^b \quad (2)$$

The constants $a = 4.47 \cdot 10^{-4}$, $b = 1.46$ and temperature $T_{ini} = 190$ °C were obtained with data from [29] and [30] by minimizing the residual sums of squares. The resulting curve and the initial data on which it was based are shown in Fig. 3.

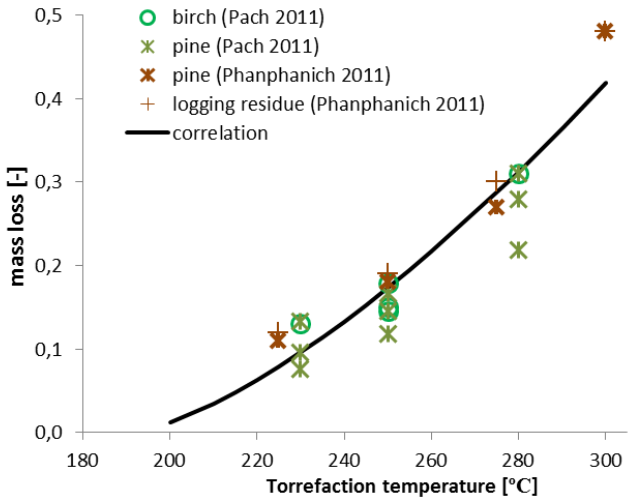

Fig. 3. Mass loss as a function of torrefaction temperature. Correlation curve represents Eq. (2).

Although softwood is known to be less reactive than hardwood, due to differences in the hemicellulose structure [27, 36], the data in Fig. 3 is too limited to clearly demonstrate this. Difference in the torrefaction time, 30 minutes by Phanphanich and Mani [30] and 1 to 3 hours by Pach et al. [29], appears to have little effect. This can be explained by the low heat conductivity of wood, meaning the temperature inside a chip changes slowly, and the fact that the mass loss rate slows after the first 20–30 minutes. Logging residues appear slightly more reactive than wood, possibly due to the higher ash content and thus greater presence of catalytic components. Overall, the correlation appears to be an adequate approximation for the mass yield of typical Scandinavian forest biomasses at >30 minute residence time and varying temperatures.

Prins et al. [3] and Prins [34] published experimental results for the gas-phase product for willow and larch, as well as some non-woody biomasses. These results were used in the thermochemical model by Bates and Ghoniem [35]. For use in this study, the data given in [3] and [34] pose some difficulties. Firstly, mass balances were not closed; the unknown rate of the missing mass leaves a significant uncertainty for the comparatively small mass fraction in the gas phase. Secondly, only the true gas-phase components are considered, but in industrial equipment solids and tar are likely to be transported out of the reactor as dust and droplets with the gas stream. These components may have heating values an order of magnitude greater than the gas, and may have a notable effect on the total heating value transported with the gas flow.

In the absence of more accurate information, the data for woody biomasses (larch and willow, approximately 10% moisture) from [3] and [34] were used to obtain a simple curve fit for the heating value of the torrefaction gas, shown in Eq. (3) and Fig. 4. Due to the limitations in material library of the IPSEpro software, this gas flow was simulated as a mixture of carbon dioxide, methane and water vapour, providing the lower heating value.

$$LHV_{TG} = 2.00 + 5.28 \cdot 10^{-5} \cdot (T_{torr} - 190\ °C)^{2.49} \quad (3)$$

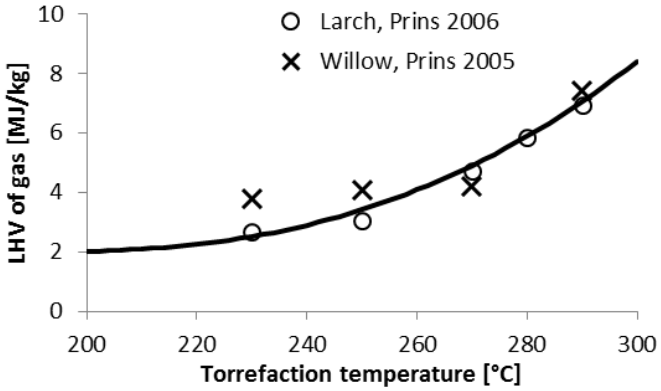

Fig. 4. Lower heating value of torrefaction gas as a function of torrefaction temperature. Experimental data from [3, 33], correlation curve represents equation (3).

Data on the heat of reaction of wood decomposition during torrefaction also suffer from a high degree of uncertainty and are partly contradictory. Bergman [4] suggests that reaction enthalpy will be within ±1% of feedstock heating value, while Prins et al. [3] measured endothermic reaction enthalpies of 87±400 kJ/kg for willow when torrefied for 30 minutes at 260 °C, and 124±449 kJ/kg for 10 minutes of torrefaction at 300 °C [36]. The stated uncertainty range, however, ignores the uncertainty resulting from failure to close the mass balances.

Recent research suggests that torrefaction reactions can be considered a two-stage process. The first stage consumes oxygen from the hemicellulose (and at higher temperatures from the cellulose) with clearly exothermic reactions. In the following stage, both endo- and exothermic reactions are present [37, 38].

Bates and Ghoniem [35] used a two-step model with three correlations to estimate the higher heating value (HHV). Regardless of the HHV correlation and torrefaction temperature, the first step reaction enthalpy always remained exothermic. The second step reaction enthalpy varied from 300 kJ/kg endothermic to -200 kJ/kg exothermic at 200 °C, depending on HHV correlation, and from -50 kJ/kg exothermic to -550 kJ/kg exothermic at 300 °C.

Ohliger et al. [39] measured heat of reaction in beech torrefaction. Results with 10% moisture beech ranged from 0…+150 kJ/kg endothermic to -150…0 kJ/kg exothermic, with the more exothermic reactions coinciding mostly with the highest mass losses, i.e. long time and/or high temperature. High moisture content caused more endothermic reactions, probably due to vapour flow flushing the volatiles needed in the exothermic second-stage reactions from the reactor [38]. Results of van der Stelt [37] also indicate a trend towards increasingly exothermic behaviour at increasing temperatures, although the results of 1.5 MJ/kg endothermic to -1.2 MJ/kg exothermic had significant uncertainty from the mass balance not being closed. Experimental co-torrefaction of hemicellulose, cellulose and lignin for 60 minutes by Chen and Kuo [38] indicated the opposite behaviour, with net exothermic reactions at 230 °C, less exothermic reactions at 260 °C, and even slightly endothermic reactions at 290 °C. Recently, Peduzzi et al. [40] estimated the heat of reaction for unspecified wood biomass at 250 °C as -170 kJ/kg exothermic, and Basu et al. [41] found a heat of reaction of -360 kJ/kg for poplar wood at unspecified temperature.

Although there appears a tendency for torrefaction to exhibit slightly exothermic heat of reaction more often than not, the data were considered too dispersed and contradictory to serve as a basis for a model that could predict accurately the change of heat of reaction as a function of temperature. A constant -500 kJ/kg$_{feed,dry}$ heat of reaction, considered a conservative estimate for determining the solid product energy yield, was used in the model. The resulting energy yield and solid matter heating value behaviour appear reasonably close to published results. The relative change of solid product dry fraction LHV (energy ratio ER [-]) and energy yield *E* [-], defined as in Eq. (4) and (5)

$$ER = \frac{LHV_{\mathrm{torr}}}{LHV_{\mathrm{d}}} \tag{4}$$

$$E = ER \cdot \frac{m_{\mathrm{torr}}}{m_{\mathrm{d}}} \tag{5}$$

are plotted as a function of torrefaction temperature together with experimental data from references [29] and [30] in Fig. 5.

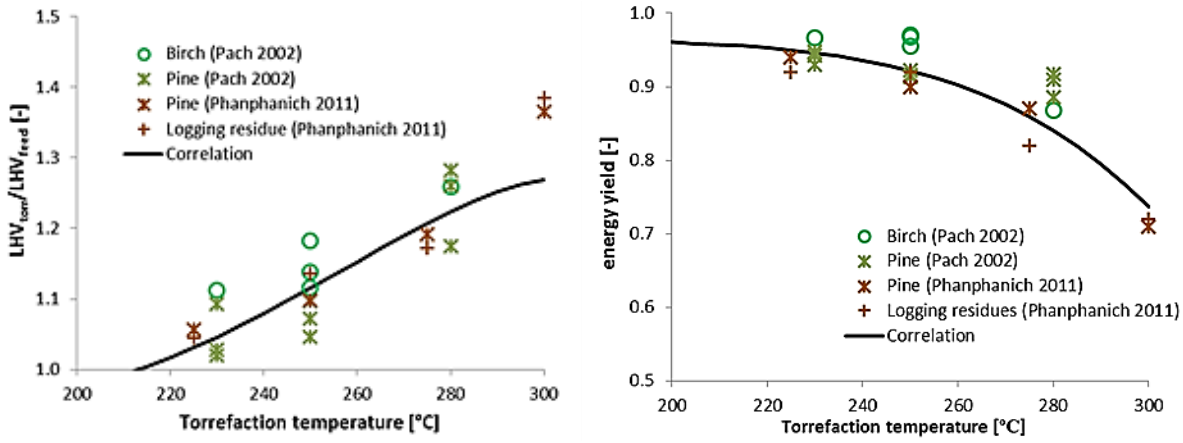

Fig. 5. Model-based solid product energy ratio (Eq. (4)) and energy yield (Eq. (5)) compared to experimental results from [29, 30].

The experimental results used for torrefaction modeling in current study are derived from laboratory-scale units. Although the presence of feedstock material with various sizes and shapes together with inevitable impurities would affect the reaction kinetics in case of industrial-scale operation, Medik et al. [42] found that this effect is less strong than temperature and residence time influence. The results of several studies indicate that larger particles would react slower, however, with sufficient reaction time these differences in behaviour become less pronounced [41, 42]. Moreover, the character of mass loss maintains somewhat the same with particle size variations [43]. Consequently, it was assumed that within the frames of existing limitations, the torrefaction model developed in current work could be applied to industrial-scale units.

2.3. Torrefaction heat requirement

Before torrefaction, the feedstock is typically dried to a moisture content of approximately 10% [4, 22]. Drying consumes most of the heat required for the whole torrefaction process. The dryer type is not specified in the model, but a belt dryer would enable flexibility in selecting the heat source and would allow use of fairly low-temperature sources [44]. A specific heat consumption of 1.2 kWh/$kg_{H2O\_evaporated}$, considered to represent a typical or conservative estimate for belt dryer heat consumption [44, 45], was assumed. Dryer heat can be supplied by flue gas, hot water, or low pressure steam.

From dried biomass storage the biomass feed is assumed to enter the torrefaction reactor at a temperature of 60 °C and moisture of 10%. The feed is then torrefied by heating it to the specified reaction temperature and maintaining the temperature for a sufficiently long period, typically 30—60 minutes. Indirect heating of the biomass was assumed in this study, allowing the use of any flow at a sufficient temperature for heat supply. Although torrefaction requires a higher temperature than drying, the total heat demand of torrefaction is much lower.

As industrial torrefaction reactors are not yet common equipment with known typical heat consumption rates, a model-based approximation had to be used. Accurate modeling of the heat consumption in torrefaction is challenging for several reasons, in particular because of variations in the specific heat of the wood, the heat of the reaction during torrefaction, and the magnitude of heat losses.

The model used in this study assumes that moisture content remains constant up to 100 °C, at which point all moisture is evaporated. The net heat consumption Φ_{TORR} [kW] in the torrefaction reactor can be considered to consist of five separate parts: 1) sensible heat of moist wood temperature change, $\Phi_{<100°C}$ [kW]; 2) latent heat of remaining evaporation, Φ_{evap} [kW]; 3) sensible heat of dry wood and water vapour, $\Phi_{100°C\text{-}Torr}$ [kW]; 4) heat of reaction in torrefaction, Φ_{react} [kW], and 5) heat losses, Φ_{loss} [kW]. The sensible heats are obtained from equations (6) and (7):

$$\Phi_{<100°C} = \dot{m}_{feed}\,\bar{c}_{p,<100°C}\left(100\,°C - T_{feed,in}\right) \quad (6)$$

$$\Phi_{100\,°C-Torr} = \dot{m}_{feed}\left(T_{torr} - 100\,°C\right)\left[\left(1 - MC_{feed}\right)\bar{c}_{p,dry} + MC_{feed}\bar{c}_{p,vapour}\right] \quad (7)$$

where MC_{feed} is the moisture content of the feedstock.

The specific heat of wood has a strong dependence on temperature [46], but shows little [47] or no dependence [48] on the wood species. Moisture also affects the specific heat. Part of the moisture is not free liquid in the cells but bound to the fibres. As a result, the net specific heat of moist wood is greater than the weighted sum of dry and water components [48]. Decomposition of wood begins at approximately 150 °C, affecting the c_p [39].The specific heat of moist wood $\bar{c}_{p,<100°C}$ [kJ/kgK] was estimated from a correlation by TenWolde [47] as cited in [47]

$$\bar{c}_{p,<100°C} = \frac{\bar{c}_{p,dry,<100°C} + 4.19 MC_{db}}{1 + MC_{db}} + MC_{db}\left(0.02355\,\bar{T} - 1.32\,MC_{db} - 6.191\right) \quad (8)$$

where MC_{db} [-] is the fractional dry basis moisture content and $\bar{T}$ [K] is the average temperature. The dry wood specific heat $\bar{c}_{p,dry,<100°C}$ [kJ/kgK] is obtained from

$$\bar{c}_{p,dry,<100°C} = 0.1031 + 0.003867 \cdot \bar{T} \quad (9)$$

The specific heat of water vapour is assumed to be 1.95 kJ/kgK. The correlation in Eq. (9) is valid for dry wood up to 147 °C, from which point onwards wood decomposition begins [39]. Other correlations for dry wood c_p also exist, up to a maximum of 177 °C, for example those by Skaar [51], Koch [52], and Gupta et al. [53]. All suggest linear dependence to absolute temperature. Harada et al. [54] presents a linear correlation up to 260 °C. This correlation, however, differs significantly from the others. At 147 °C all correlations are within 0.25 kJ/kgK, but when extrapolated to torrefaction temperatures the range increases to almost 0.57 kJ/kgK at 300 °C.

Ohliger et al. [39] considered taking the c_p above 147 °C to be either that of char or an average of that of char and extrapolated wood c_p. However, char has a much lower c_p than wood, and given the relatively short duration of the heating phase, in this paper the properties were assumed to be much closer to those of wood than char. In the absence of a more accurate model, Eq. (9), yielding lowest c_p of the compared correlations, with the exception of that of Harada [54], was used also in the range of 147 °C < T < 300 °C, with the knowledge that considerable errors may thus be introduced.

The heat required for the evaporation of the last moisture from the wood was calculated from

$$\Phi_{evap} = \dot{m}_{feed}\, MC_{feed}\, h_{fg} \quad (10)$$

where a value of of h_{fg} = 2260 kJ/kg, corresponding to the latent heat of evaporation of free water at 100 °C, was assumed, ignoring the effect of bound moisture. The error thus introduced was assumed to be small and most likely of opposite direction compared to the error caused by the extrapolation of dry wood c_p.

Although the bulk of published data indicates somewhat exothermic heat of reaction, which was also assumed for determining the solid product heating value, the data can still be considered varied and sometimes contradictory. To avoid an overly optimistic estimate of the heating benefit from the exothermicity of the reactions, h_{react} was thus assumed to be zero when determining the heating requirement.

Some heat losses from the reactor are inevitable during the process. However, without considering the design of the reactor, it is hard to evaluate them properly. In current model this loss was assumed to be 10% of the total heat requirement.

Figure 6 shows the total heat consumption of torrefaction reactor at three different temperatures and 10% moisture feedstock at a temperature of 60 °C. The heat consumption of drying the chips from 50% to 10% is also indicated for comparison. It is evident from the figure that water evaporation accounts for the vast majority of the energy demand in torrefaction, most of it in the dryer.

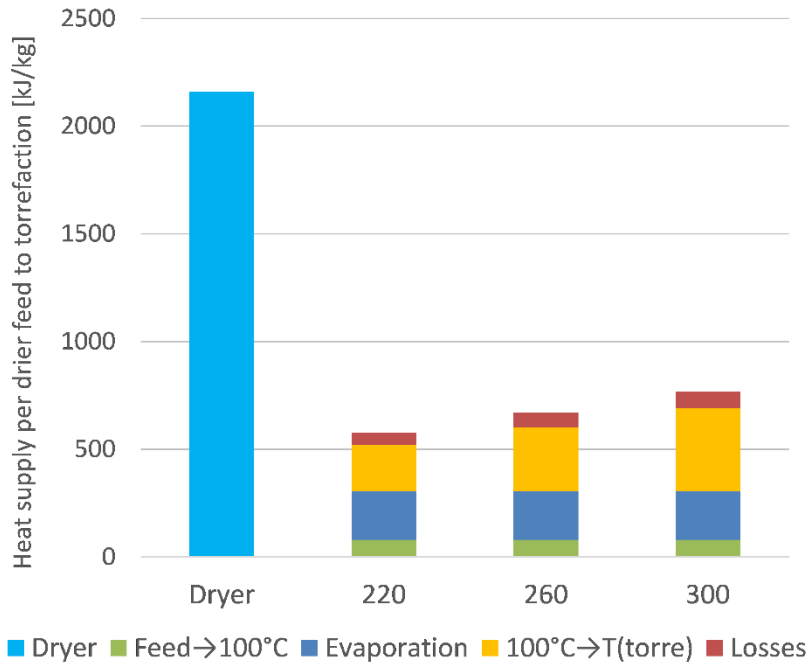

Fig. 6. Heat consumption of dryer and torrefier at three torrefaction temperatures [°C].

The heat requirement and energy recovery available from the torrefaction process are illustrated in Fig. 7. While at low temperatures the process is a clear net consumer of energy, as torrefaction severity increases, the gas stream volume and heating value increase rapidly, reaching the process heat need at 300 °C. The sensible heat recovered from the process is negligible in comparison.

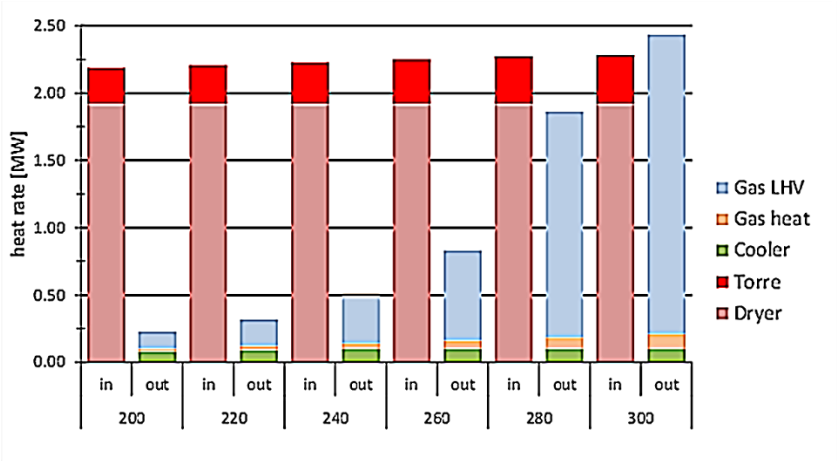

Fig. 7. Energy required and recovery of torrefaction process (1 kg/s feedstock with wet basis moisture content of 50%).

3. INTEGRATION OF TORREFACTION AND COGENERATION PLANTS

3.1. CHP plant models

Two different CHP plants were considered for the integration analysis: a large-scale biomass fired plant with a 385 MW circulating fluidized bed (CFB) boiler and a condensing turbine [55], henceforth referred to as Plant A, and a smaller biomass fired backpressure plant with a 29 MW bubbling fluidized bed (BFB) boiler [56] (Plant B). Both plants are based on actual operating industrial plants and their performance has been modeled using IPSEpro software. They are assumed to run on the basis of required heat demand; integration of torrefaction will thus affect only electricity production and fuel consumption.

Plant A produces 103 MW electricity and 110 MW district heat at 90/50 ºC supply/return temperature levels during the three month winter peak. In addition, 120 MW of process steam is supplied continuously for industrial purposes at 16.5 bar(a), 10 bar(a) and 4.5 bar(a) pressures. This type of plant is usually built to produce electricity. So, the assumption used for choosing the operation type for Plant A tries to run at maximum steam load while operating. As the plant tries to run at full boiler load, the condensing tail takes whatever steam remains after the steam extractions for thermal load fulfilment.

Plant B is an example of a small CHP plant that is typically utilized, e.g. in central Europe, to increase small-scale heat and power production from biomass. At full load it produces 7.9 MW electricity and 20.0 MW district heat. A different scenario is considered with this plant because this kind of plant is typically built to fulfil district heating demand. When the heat load of a backpressure plant is decreased (spring/autumn season), the steam flow through the turbine and therefore electricity output are inevitably reduced. Under these circumstances, an additional heat consumer in the form of a torrefaction plant can increase the electricity output by using the available free boiler capacity. In this study, a case of 60% district heat load (12 MW) at 90/50 ºC temperature level was chosen to represent typical reduced-load conditions.

The main plant parameters at full load design point operation are summarized in Table 1; schematic diagrams of the design cases are shown in Fig. 8 and Fig. 9. For the wood chips used both as boiler fuel and torrefaction feedstock, a moisture content of MC = 50% and lower heating value of 18.8 MJ/kg on a dry basis were assumed based on data from Alakangas [57]. For both cases, the torrefied solid fuel could be either used internally, processed further in the plant, for example, by pelletizing, or sold on the market as torrefied chips; the scope of this study was limited to the integration of the torrefaction and CHP processes.

Table 1.
Main characteristics of CHP plants at full load design point.

Category	Parameter	Plant A	Plant B
Net production	Electricity	103 MW	7.9 MW
	District heat	110 MW	20.0 MW
	Process heat	120 MW	-
Boiler	Type	CFB	BFB
	Thermal output	385 MW	29 MW
	Stack temperature	150 °C	150 °C
Turbine	Inlet steam	110 bar / 550 °C	90 bar / 500 °C
	Back pressure (DH)	0.4 bar	0.8 bar
	Condenser pressure	50 mbar	n/a
	Extractions	50*/16.5/10/4.5 bar(a)	59*/8.5 bar(a)
Main losses	Boiler	55 MW	4.3 MW
	Condenser	37 MW	n/a
	Auxiliary power	8.1 MW	0.60 MW

* To obtain high-pressure steam for torrefaction, it is assumed that an extraction can be created in the settling chamber after the partial admission control stage at the turbine inlet.

Solid fuel Air Flue gases Steam Water Condensate Cooling water
DH condenser– district heating condenser; *LUVO* – air preheater; *Preheater* – feed water preheater; *SH* – superheater; *SCAH* – steam coil air preheater

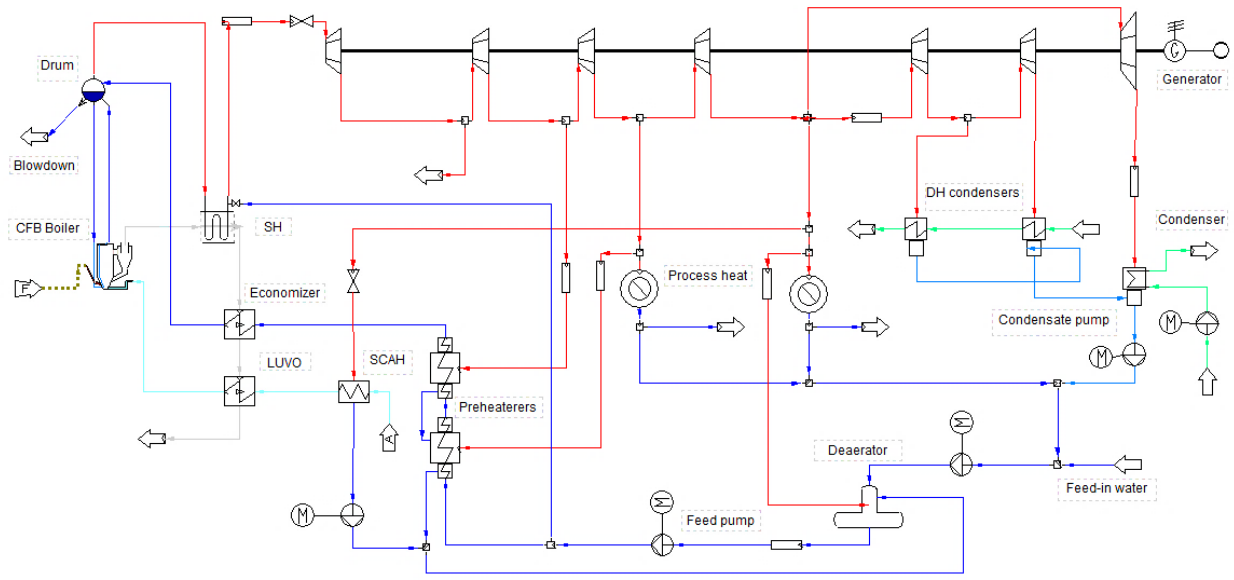

Fig. 8.
Design case model for Plant A.

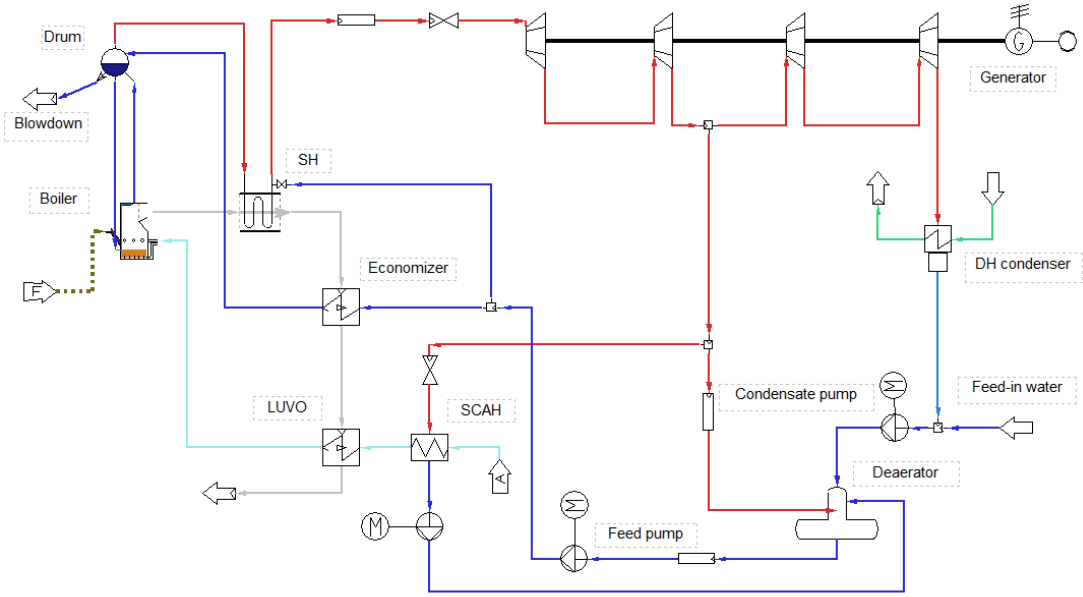

Fig. 9. Design case model for Plant B.

The boiler for both cases is modelled using four components: the furnace, including the steam drum, followed by a series of three heat exchangers in the flue gas flow direction, representing the superheater, economizer and air preheater. Heat transfer rate Φ [kW] in the three heat exchangers is determined from

$$\Phi = G\Delta T_{\mathrm{lm}} \tag{11}$$

where the conductance G [kW/K] is the product of the overall heat transfer coefficient U [kW/m^{2}K] and heat transfer area A [m^2], and ΔT_{lm} [K] is the logarithmic temperature difference. Table 2 lists the values for design point conductance G of the main heat transfer surfaces for both plants.

Table 2. Heat transfer surface conductance [kW/K] of boilers at design point.

Heat transfer surface	Plant A	Plant B
Steam generator	260	n/a
Superheater Economizer	420	26
Air preheater	500	32
Steam coil air preheater	640	34
	20	5

Component performance changes in off-design conditions. In this study, variations in turbine and pump isentropic efficiencies were assumed to remain small and not considered. In the boiler, the conductances *G* of the superheater, economizer and air preheater are assumed to change in proportion to relative gas flow change [58]:

$$G = G_0 \left(\frac{\dot{m}_{\mathrm{FG}}}{\dot{m}_{\mathrm{FG},0}} \right)^{0.6} \tag{12}$$

where $\dot{m}_{FG}$ is the flue gas mass flow rate, with subscript 0 referring to the design point.

A steam coil air preheater is used to prevent flue gases from cooling below 150 °C. In some cases, the stack temperature may increase slightly above 150 °C. Full superheat can be maintained by reducing the water injection to superheater in most cases, but in some situations, especially with the smaller plant at part load, the live steam temperature will inevitably be slightly reduced.

With reduced loads, the auxiliary power consumption P_{aux} also drops. Part-load P_{aux} is estimated from:

$$P_{\mathrm{aux}} = \left(0.5 + 0.25 \frac{\dot{m}_{\mathrm{FG}}}{\dot{m}_{\mathrm{FG},0}} + 0.25 \frac{\dot{m}_{\mathrm{FW}}}{\dot{m}_{\mathrm{FW},0}} \right) P_{\mathrm{aux},0} \tag{13}$$

where $\dot{m}_{\mathrm{FW}}$ is the feed water flow rate, with subscript 0 referring to the design point.

3.2. Integration options

The heat required for the torrefaction process can be provided by various streams, such as hot water, flue gases from the boiler, or steam from the turbine. The thermodynamic performances of six different integration schemes (Table 3) were investigated. Case 0 represents a non-integrated operation of the CHP plant and torrefaction unit and was used as a reference point for comparison. In Case 0, the heat demand of the torrefier and dryer was supplied by flue gases from the combustion of torrefaction gas and additional fuel. In all cases studied, power consumption of the torrefaction process was assumed to be $200 kW / \dot{m}_{H_2O,evap}$ in the dryer, $50 kW \cdot \dot{m}_{in}$ in the torrefier, and $200 kW \cdot \dot{m}_{feed}$ for the total sum of power consumption of other components.

Table 3. Heat sources for torrefaction process units.

	Heat source for section	
Case	Torrefaction	Drying
Case 1	saturated water from the drum	water after the torrefier
Case 2	saturated water from the drum	flue gases after air preheater
Case 3	flue gases after the superheater	flue gases after the torrefier
Case 4	flue gases after the superheater	backpressure steam
Case 5	steam extraction from the HP turbine	backpressure steam
Case 6	steam extraction from the HP turbine	steam after the torrefier

In Cases 1 and 2, the water from the boiler drum is returned back to the steam-water system after supplying heat for the torrefaction process units. The temperature of the exhaust gases after the dryer for Cases 2 and 3 was set at 150 °C. In Case 4, flue gases are returned back to the boiler after the torrefier. Condensate from the dryer in Cases 4, 5 and 6 is mixed to the main condensate flow before the deaerator.

The following assumptions were applied to all cases:

- Heat from the torrefied biomass cooling is used for combustion air preheating;
- For all integration cases the torrefaction gas is co-fired in the boiler together with biomass;
- Torrefaction heat losses are independent of the heating media used;
- Live steam pressure is fixed at the design level;
- Constant mass flow of solid biomass to torrefaction is assumed (10 kg/s for Plant A and 1 kg/s for Plant B integration cases)

To compare the performance of the considered schemes, the trigeneration efficiency [%] was calculated:

$$\eta_{\text{trig}} = \frac{(P_{\text{gen}} - \sum P_{\text{pump}} - \sum P_{\text{aux}}) + (Q_{\text{DH}} + Q_{\text{process}}) + \dot{m}_{\text{torr}} \cdot LHV_{\text{torr}}}{\dot{m}_{\text{tot\_fuel}} \cdot LHV_{\text{fuel}}} \cdot 100\% \quad (14)$$

where P_{gen} is the power at the generator terminals [MW]; ΣP_{pump} is the electric power consumed by the pumps in the steam cycle (feed water pump and condensate pump) [MW]; ΣP_{aux} is the power used by other plant equipment (fans, fuel and ash handling, etc.); Q_{DH} is the district heating load [MW]; Q_{process} is the process heat [MW]; $\dot{m}_{\text{torr}}$ [kg/s] is the mass flow rate of torrefied fuel; $\dot{m}_{\text{tot\_fuel}}$ [kg/s] is the combined mass flow rate of boiler solid fuel and torrefaction feedstock; and LHV_{fuel} and LHV_{torr} are the lower heating values of untreated and torrefied solids respectively [MJ/kg].

3.3. Simulation results and discussion

Figure 10 illustrates solid fuel consumption as a function of torrefaction temperature for the studied integration cases. The solid fuel consumption reduces with increasing torrefaction temperature for both the large and the small CHP plant. This result is as expected since the higher the torrefaction temperature the greater is the mass loss at torrefaction. Thus, both the heating value and the mass flow rate of the torrefaction gases to the boilers increase with increased torrefaction temperature. As a result, a larger share of solid fuel can be substituted in the boiler. The increase in torrefaction reactor heat consumption (about 40% more for the highest temperature level than for the lowest one) is negligible in comparison.

When the boiler of Plant A is operated at full load, increasing the share of torrefaction gas that is co-fired leads to growing economy of the main solid fuel use (Fig. 10 (a)). In Cases 2 and 3, the relatively high heat demand of the dryer is covered by the heat of flue gases. Under these circumstances, the heat of flue gasses is not sufficient to maintain the necessary level of combustion air preheating in air-preheater. The steam coil with increased heat transfer area is used to fulfil the required air preheating. As a result of decreased heat transfer rate of air-preheater, the fuel mass flow rate to the boiler decreases. Case 2 demonstrates the highest decrease in fuel consumption among the integration cases: a 7.5% increase in fuel economy for the 300 °C torrefaction temperature in comparison with the non-integrated case. Case 3 achieves a 6.1% increase in fuel economy at the same conditions. Cases 1, 4, 5 and 6 exhibit virtually identical numbers within the studied temperature range (from 0.2% at the lowest temperature level to 5.4% increase in fuel economy at the highest temperature).

With regard to Plant B, the solid fuel consumption for all integration cases is higher in comparison with the design case (Fig. 10 (b)). Similarly to integration options for Plant A, Cases 2 and 3, where heat from flue gasses is captured to torrefaction, behave noticeably differently from the other cases. Maintaining the combustion air temperature at the required level in these two cases leads to increased steam mass flow through the steam coil. As a result, mass flow of live steam and boiler fuel to produce it also increase. At the lowest temperature level, Cases 1, 4, 5 and 6 have fuel consumption that is 12% – 17% higher than the design values, and the fuel consumption gets relatively close to the design case consumption at 300 °C. Whereas cases 2 and 3 have an average increase of 38.1% and 46.1% respectively.

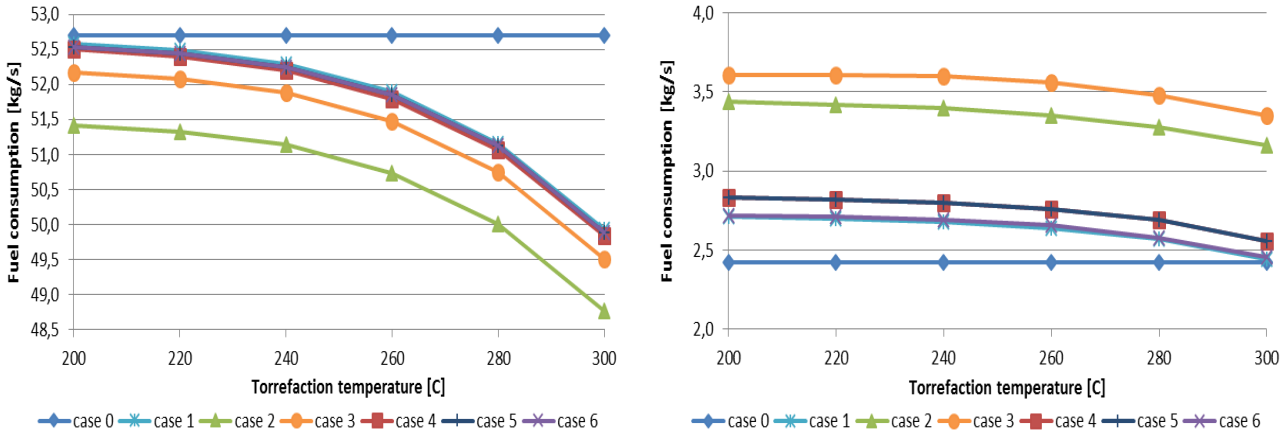

(a) (b)

Fig. 10. Solid fuel consumption for Plant A (a) and Plant B (b) integration cases.

Power generation for both plants varies slightly with torrefaction temperature. The way of integration, however, has a rather strong effect. Averaged over the temperature range, the net power output at different integration cases for both plants is presented in Fig. 11. The power production of the larger Plant A is reduced when torrefaction is introduced, since the torrefaction heat demand either decreases steam production, or some of the generated steam needs to be extracted before expansion to condenser pressure. Heat that is taken from the boiler for torrefaction reduces the live steam mass flow to the turbine in Cases 1, 2 and 3, and as a consequence, electricity output is decreased: respectively 9.4%,

11% and 10%, compared to electricity production in the non-integrated plant. Another factor is the necessary level of air preheating that needs to be maintained by the steam coil in Cases 2 and 3. Higher consumption of steam results in a bigger loss of net power output for these two cases. In Cases 4 and 5, the boiler steam production is relatively close to the design value, and steam energy from the final expansion to condenser pressure is only lost due to torrefaction. Therefore, the reduction in power output is lowest in these two cases: correspondingly, 3.2% and 1.1% lower in comparison with the base Case 0.

A quite different situation is observed with the smaller Plant B integration options. The available free capacity of the boiler allows increase in power output for almost all integration cases. In order to fulfil the higher demand for steam mass flow to air preheating, steam mass flow through the turbine and, as a result, net electricity output increase significantly in Cases 2 and 3 (43.4% and 50.7% more than in the design case). In Case 6, meeting the heat demand of the dryer and torrefier with high pressure steam results in a loss of generation power. For this reason, the net power output for this case is 5.1% lower than the design value.

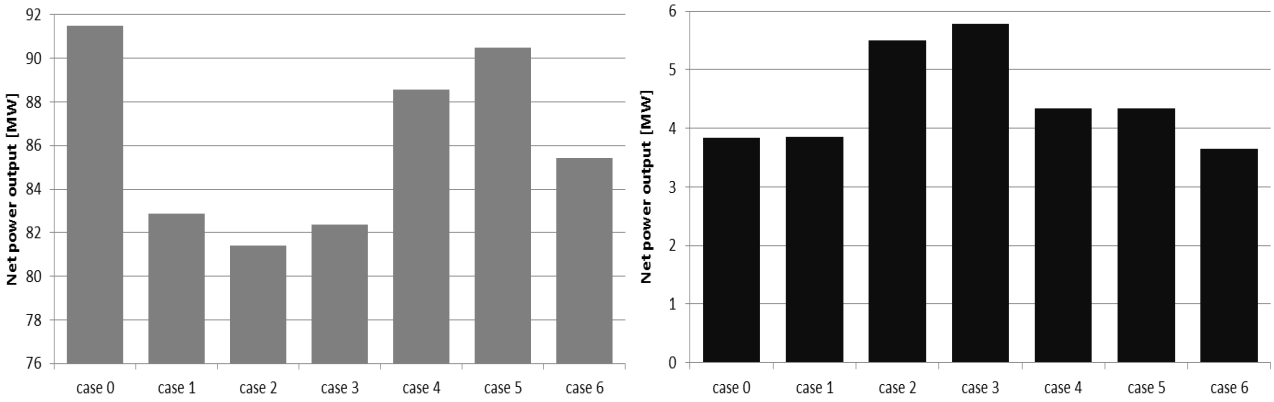

(a) (b)

Fig. 11. Net power output averaged over torrefaction temperature range (200–300 ºC) for Plant A (a) and Plant B (b) integration cases.

The impact of the chosen integration scheme and torrefaction temperature on trigeneration efficiency (Eq. (13)) is presented in Fig. 12. The amount of low-value heat that is produced and basically lost in the condenser decreases in Plant A quite significantly in all integration cases in comparison with the design case. As a consequence of the reduction of this loss in the overall plant balance, the trigeneration efficiency for all integration options is notably higher than in Case 0 (Fig. 12 (a)). However, with the considerable decrease of torrefied fuel mass flow at high temperatures, trigeneration efficiency curves for all cases slope downwards. Of the integration options studied, Case 5 has the highest efficiency: on average 5.2% higher than the design case.

In Plant B, the impact of the increased fuel mass flow exceeds the effect of greater power generation; as a consequence, the trigeneration efficiency for most of the cases is lower than for the reference Case 0 (Fig. 12 (b)). The efficiency changes within a relatively narrow range close to the design level for most of the cases studied (from 0.4% loss on average for Cases 4, 5 and 6 to 0.9% increase for Case 1). For Cases 2 and 3, the increased amount of steam for air preheating leads to higher steam mass flow through the turbine. Since this would increase the district heat production above the specified 12 MW, an auxiliary cooler to dump the excess heat from the DH network needed to be utilized in these cases. As a consequence of this additional heat loss in the energy balance of the plant, the lowest values for trigeneration efficiency are found in Cases 2 and 3: 9.7% and 12.2% lower than in the design case.

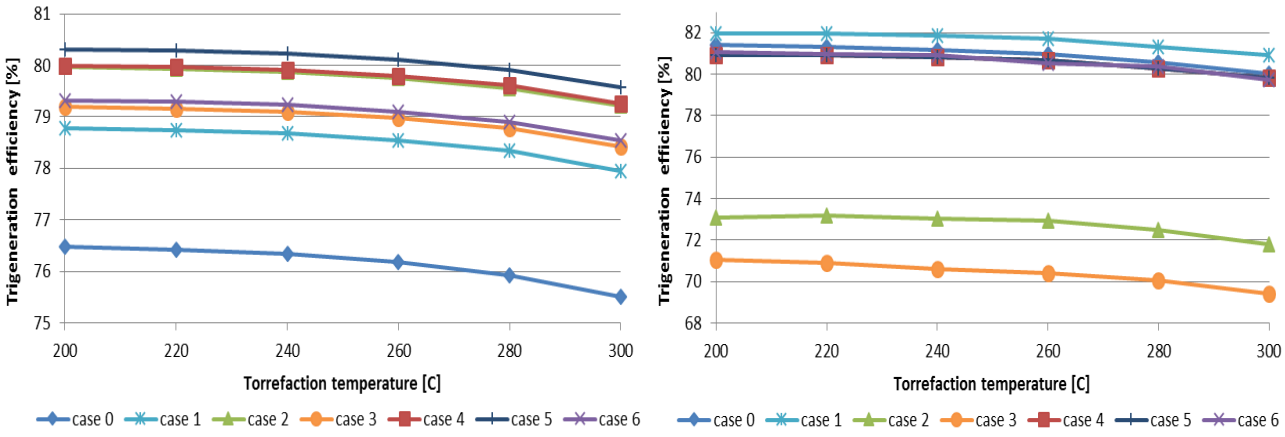

(a) (b)

Fig. 12. Trigeneration efficiency for Plant A (a) and Plant B (b) integration cases calculated with Eq. (14).

4. Conclusions

In order to investigate the effect of torrefaction process on power plant cycle, the torrefaction model was developed and then integrated with models of two different-sized CHP plants. The first plant represented an example of a large-scale plant operated at full boiler load, while the second model was a smaller backpressure plant operated mostly at a reduced district heating load. Six integration concepts were implemented for both plants and the performance of the integrated plants was evaluated within the typical range of torrefaction temperatures.

The operation assumptions used in this work led to quite different results for the studied integration options. With the larger plant, maintaining maximum boiler output and simultaneous co-firing of torrefaction gas decrease fuel consumption and power output with torrefaction temperature increase. As for the smaller boiler at partial load operation, the fuel consumption was somewhat higher than in the design case, while increased steam flow led to additional electricity output. The efficiency of the feedstock conversion into useful energy streams (trigeneration efficiency) is determined mostly by the type of integration and differs only slightly with torrefaction temperature. The trigeneration efficiency for all integration options with the first plant is higher than for the non-integrated case. As for the second plant, the effect of the integration is relatively low for most of the studied cases. For both plants, the integration cases that used the heat of flue gases for torrefaction performed quite differently than the other studied scenarios: capture of a certain amount of heat from flue gases resulted in additional consumption of steam for the combustion air preheating.

The results of the simulations indicate the diverse effect of the various integration scenarios on the performance of CHP plants operated under different regimes. As expected, torrefaction parameters have an effect on integration performance: at higher torrefaction temperatures a larger share of fuel can be substituted with torrefaction gas. Based on the analysis presented in this study, it can be concluded that the potential of integration of torrefaction with a cogeneration plant is highly dependent on the operation characteristics of both the CHP plant and the torrefaction process and each particular case requires individual evaluation from the point of view of both reduction in fuel consumption and additional cost analysis.

References

1. Van der Stelt M, Gerhauser H, Kiel JHA, Ptasinski KJ. Biomass upgrading by torrefaction for the production of biofuels: A review. Biomass Bioenerg 2011; 35: 3748–62. http://dx.doi.org/10.1016/j.biombioe.2011.06.023
2. Verhoeff F, Adell A, Boersma AR, Pels JR, Lensselink J, Kiel JHA, et al. TorTech: Torrefaction as key technology for the production of (solid) fuels from biomass and waste. ECN Biomass, Coal and Environmental Research, Report ECN-E--11-039; 2011.
3. Prins MJ, Ptasinski KJ, Janssen FJ. Torrefaction of wood. Part 2. Analysis of products. J Anal Appl Pyrol 2006; 77: 35–40. http://dx.doi.org/10.1016/j.jaap.2006.01.001
4. Bergman PCA, Boersma AR, Zwart RWR, Kiel JHA. Torrefaction for biomass co-firing in existing coal-fired power stations. ECN, Report ECN-C--05-013, Netherlands; 2005.

5. Uslu A, Faaij AP, Bergman PCA. Pre-treatment technologies, and their effect on international bioenergy supply chain logistics. Techno-economic evaluation of torrefaction, fast pyrolysis and pelletisation. Energy 2008; 33:1206–33. http://dx.doi.org/10.1016/j.energy.2008.03.007
6. Pirraglia A, Gonzalez R, Saloni D, Denig J. Technical and economic assessment for the production of torrefied ligno-cellulosic biomass pellets in the US. Energ Convers Manage 2013; 66: 153–164. http://dx.doi.org/10.1016/j.enconman.2012.09.024
7. Cocchi M, Nikolaisen L, Junginger M, Goh CS, Heinimö J, Bradley D. Global Wood Pellet Market Study 2011; IEA Bioenergy.
8. Lamers P, Junginger M, Hamenlick C, Faaij A. Developments in international solid biofuel trade. An analysis of volumes, policies, and market factors. Renew Sust Energ Rev 2012; 16(5): 3176–99. http://dx.doi.org/10.1016/j.rser.2012.02.027
9. IEA. Technology roadmaps: International Energy Agency (IEA), IEA; 2010.
10. Directive 2012/27/EU of European Parliament and of the Council. Official Journal of the European Union 2012, L 315/1.
11. Biomass co-firing. Technology brief. IEA-ETSAP and IRENA Technology Brief E21; 2013.
12. Koppejan J, Sokhansanj S, Melin S, Madrali S. Status overview of torrefaction technologies. IEA Bioenergy Task 32 report 2012, Enschede.
13. Eriksson G, Kjellström B. Assessment of combined heat and power (CHP) integrated with wood-based ethanol production. Appl Energ 2010; 87(12): 3632–41. http://dx.doi.org/10.1016/j.apenergy.2010.06.012
14. Ilic D, Dotzauer E, Trygg L. District heating and ethanol production through polygeneration in Stockholm. Appl Energ 2012; 91(1): 214–221. http://dx.doi.org/10.1016/j.apenergy.2011.09.030
15. Starfelt F, Daianova L, Yan J, Thorin E, Dotzauer E. The impact of lignocellulosic ethanol yields in polygeneration with DH—a case study. Appl Energ 2012; 92: 791–9. http://dx.doi.org/10.1016/j.apenergy.2011.08.031
16. Starfelt F, Thorin E, Dotzauer E, Yan J. Performance evaluation of adding ethanol production into an existing combined heat and power plant. Bioresource Technol 2010; 101(2): 613–18. http://dx.doi.org/10.1016/j.biortech.2009.07.087
17. Zhou W, Yang H, Rissanen M, Nygren B, Yan J. Decrease of energy demand for bioethanol-based polygeneration system through case study. Appl Energ 2012; 95: 305–11. http://dx.doi.org/10.1016/j.apenergy.2012.02.014
18. Brammer J, Bridgewater A. Drying technologies for an integrated gasification bio-energy plant. Renew Sust Energ Rev 1999; 3(4): 243–89. http://dx.doi.org/10.1016/S1364-0321(99)00008-8
19. Difs K, Wetterlund E, Trygg L, Söderström M. Biomass gasification opportunities in a DH system. Biomass Bioenerg 2010; 34(5): 637–51. http://dx.doi.org/10.1016/j.biombioe.2010.01.007
20. Fahlén E, Ahlgren E. Assessment of integration of different biomass gasification alternatives in DH systems. Energy 2009; 88(5): 2184–95. http://dx.doi.org/ 10.1016/j.energy.2008.10.018
21. Wahlund B, Yan J, Westermark M. A total energy system of fuel upgrading by drying biomass feedstock for cogeneration: a case study of Skellefteå bioenergy combine. Biomass Bioenerg 2002; 23(4): 271–81. http://dx.doi.org/10.1016/S0961-9534(02)00055-7
22. Kohl T, Laukkanen T, Järvinen M, Fogelholm C-J. Energetic and environmental performance of three biomass upgrading processes integrated with a CHP plant. Appl Energ 2013; 107:124–34. http://dx.doi.org/10.1016/j.apenergy.2013.02.021
23. Håkansson K, Nordin A, Nordwaeger M, Olofsson I, Svanberg M. Process and system integration aspects of biomass torrefaction. 18th European Biomass Conference and Exhibition proceedings, Lyon, France; 2010.
24. Li J, Brzdekiewicz A, Yang W, Blasiak W. Co-firing based on biomass torrefaction in a pulverized coal boiler with aim of 100% fuel switching. Appl Energ 2012; 99: 344–54. http://dx.doi.org/10.1016/j.apenergy.2012.05.046
25. IPSEpro 4.0. © 1997–2015 SimTech GmbH.
26. Bergman PC, Kiel JH. Torrefaction for biomass upgrading. 14th European Biomass Conference proceedings, Paris, France; 2005.
27. Prins MJ, Ptasinski KJ, Janssen FJ. Torrefaction of wood. Part 1. Weight loss kinetics. J Anal Appl Pyrol 2006; 77: 28–34. http://dx.doi.org/10.1016/j.jaap.2006.01.002
28. Repellin V, Govin A, Rolland M, Guyonnet R. Modelling anhydrous weight loss of wood chips during torrefaction in a pilot kiln. Biomass Bioenerg 2010; 34: 602–9. http://dx.doi.org/10.1016/j.biombioe.2010.01.002
29. Pach M, Zanzi R, Björnbom E. Torrefied biomass: A substitute for wood and charcoal. 6th Asia-Pacific International Symposium on Combustion and Energy Utilization proceedings, Kuala Lumpur; 2002.
30. Phanphanich M, Mani S. Impact of torrefaction on the grindability and fuel characteristics of forest biomass. Bioresource Technol 2011; 102: 1246–53. http://dx.doi.org/10.1016/j.biortech.2010.08.028

31. Larsson SH, Rudolfsson M, Nordwaeger M, Olofsson I, Samuelsson R. Effects of moisture content, torrefaction temperature, and die temperature in pilot scale pelletizing of torrefied Norway spruce. Appl Energ 2013; 102: 827–32. http://dx.doi.org/10.1016/j.apenergy.2012.08.046
32. Bridgeman T, Jones J, Shield I, Williams P. Torrefaction of reed canary grass, wheat straw and willow to enhance solid fuel qualities and combustion properties. Fuel 2008; 87(6): 844–56. http://dx.doi.org/10.1016/j.fuel.2007.05.041
33. Felfli FF, Luengo CA, Suárez JA, Beatón PA. Wood briquette torrefaction. Energy for Sustain Dev 2005; 9(3): 19–22. http://dx.doi.org/10.1016/S0973-0826(08)60519-0
34. Prins MJ. Thermodynamic analysis of biomass gasification and torrefaction [dissertation]. Eindhoven: Technical University of Eindhoven; 2005.
35. Bates RB, Ghoniem AF. Biomass torrefaction: Modelling of reaction thermochemistry. Bioresource Technol 2013; 134: 331-40. http://dx.doi.org/10.1016/j.biortech.2013.01.158
36. Prins MJ, Ptasinski KJ, Janssen FJJG. More efficient biomass gasification via torrefaction. Energy 2006; 31(15): 3458-70. http://dx.doi.org/10.1016/j.energy.2006.03.008
37. Van der Stelt MJC. Chemistry and reaction kinetics of biowaste torrefaction [dissertation]. Eindhoven: Technical University of Eindhoven; 2011.
38. Chen W-H, Kuo P-C. Torrefaction and co-torrefaction characterization of hemicellulose, cellulose and lignin as well as torrefaction of some basic constituents in biomass. Energy 2011; 36: 803-11. http://dx.doi.org/10.1016/j.energy.2010.12.036
39. Ohliger A, Förster M, Kneer R. Torrefaction of beechwood: a parametric study including heat of reaction and grindability. Fuel 2013; 104: 607-13. http://dx.doi.org/10.1016/j.fuel.2012.06.112
40. Peduzzi E, Boissonnet G, Haarlemmer G, Dupont X, Marechal F. Torrefaction modelling for lignocellulosic biomass conversion processes. Energy 2014; http://dx.doi.org/10.1016/j.energy.2014.03.086
41. Basu P, Sadhukhan AK, Gupta P, Rao S, Dhungana A., Acharya B. An experimental and theoretical investigation on torrefaction of a large wet wood particle. Bioresource Technol 2014; 159: 215-22. http://dx.doi.org/ 10.1016/j.biortech.2014.02.105
42. Medic D, Darr M, Shah A, Rahn S. The effects of particle size, different corn stover components, and gas residence time on torrefaction of corn stover. Energies 2012; 5: 1199-1214. http://dx.doi.org/10.3390/en5041199
43. Kokko L. A method for finding suitable particle sizes for thermal conversion processes by using a simulation tool focusing on wood particle heat transfer and chemical kinetics [dissertation]. Tampere: Tampere University of Technology; 2014.
44. Arpiainen V, Wilén C. Report on optimisation opportunities by integrating torrefaction into existing industries. Deliverable No. D3.2, Production of Solid Sustainable Energy Carriers from Biomass by Means of Torrefaction. SECTOR project, EU 7th Framework Programme; 2014.
45. Fagernäs L, Brammer J, Wilén C, Lauer M, Verhoeff F. Drying of biomass for second generation synfuel production. Biomass Bioenerg 2010, 34(9): 1267–77. http://dx.doi.org/10.1016/j.biombioe.2010.04.005
46. Thunman H, Niklasson F, Johnsson F, Leckner B. Composition of Volatile Gases and Thermochemical Properties of Wood for Modeling of Fixed or Fluidized Beds. Energ Fuel 2001,15:1488-97. http://dx.doi.org/ 10.1021/ef010097q
47. Dupont C, Chiriac R, Guillaume G, Toche F. Heat capacity measurements of various biomass types and pyrolysis residues. Fuel 2014, 115: 644-51. http://dx.doi.org/10.1016/j.fuel.2013.07.086
48. Goss WP, Miller RG. Thermal Properties of Wood and Wood Products. Proceedings of Thermal performance of the exterior envelopes of buildings, V: 193-203, Atlanta, GA: ASHRAE; 1992.
49. Ragland KW, Aerts DJ. Properties of Wood for Combustion Analysis. Bioresource Technol 1991, 37:161-8.
50. TenWolde A, McNatt JD, Krahn L. Thermal properties of wood panel products for use in buildings. USDA Forest Products Laboratory, DOE/USDA-21697/1; Madison, USA; 1988.
51. Skaar C. Wood-Water Relations, Springer-Verlag, Berlin, Germany; 1988.
52. Koch P. Specific heat of oven dry spruce, pine wood and bark. Wood Science 1969; 1: 203–14.
53. Gupta M, Yang J, Roy C. Specific heat and thermal conductivity of softwood bark and softwood char particles. Fuel 2003; 82: 919-27. http://dx.doi.org/10.1016/S0016-2361(02)00398-8
54. Harada T, Hata T, Ishihara S. Thermal constants of wood during the heating process measured with the laser flash method. J Wood Sci 1998; 44(6): 425-31.
55. Ikonen O. Biomvoimalaitoksen energiatehokkuuden parantaminen ja osakuorma-ajon optimointi [master's thesis]. Lappeenranta: Lappeenranta University of Technology; 2013. Finnish.
56. Komulainen S. Voimalaitoksen käytönaikaisen optimoinnin määrittely [master's thesis]. Lappeenranta: Lappeenranta University of Technology; 2012. Finnish.
57. Alakangas E., 2000. Suomessa käytettävien polttoaineiden ominaisuuksia., VTT tiedotteita 2045. VTT Energia, Valtion Teknillinen Tutkimuskeskus, Espoo; 2000. Available at: <http://www.vtt.fi/inf/pdf/tiedotteet/2000/T2045.pdf> [Accessed April 15th, 2014].

58. Basu P. Combustion and gasification in fluidized beds. CRC Press; 2006.